Crystallographic texture configured by laser powder bed fusion additive manufacturing process: a review and its potential application to adjust mechanical properties of metallic products

Willy Ank de Morais [1,2*]
Fernando José Gomes Landgraf [2]

Abstract

The performance of engineering materials depends on the conciliation between their structure defined by the fabrication process and the properties required for their application. Within this context, the new developments in the additive manufacturing (AM) process offer great potential to generate new applications and to induce technological innovations with engineering materials. One of these innovations is the possibility of using the crystallographic texture to control proprieties that normally would not be adjustable by other mechanisms, but which are needed in certain specific applications, such as low stiffness for metallic implant parts. In this way, this article presents a structured review to describe trends in production parameters of AM by LPBF process suitable to obtain and control crystallographic texture aiming to improve the property-performance relationship of metallic materials. The increasing evolution of AM by LPBF technology is generating opportunities to increase control over texture and thus over texture-dependent properties of metallic materials products. Despite the potential of tailoring material properties by texture control, the practical use of this technique in AM by LPBF processes is still incipient.

Keywords: Additive manufacturing; Microstructure control; Crystalline texture; Stiffness.

1 Introduction

The crystallographic texture is characterized by an alignment of the material forming crystals (or grains) where a specific <*uvw*> direction is parallel to a macroscopic direction of the sample, that also can present certain crystalline planes *(hkl)* parallel to a reference plane of the sample [1,2]. This alignment creates anisotropy in material properties that can be targeted to improve component performance in specific applications. However, the induction of a crystalline orientation strong enough to obtain a relevant crystallographic texture depends on some specific phenomena. These phenomena may or may not be combined in such a way as to generate texture throughout the entire volume of the material or at certain positions [3-5], as shown in Figure 1a for a high-performance turbine blade and in Figure 1b for a bone plate implant [6].

In the case of turbine blade (Figure 1a), the portion of the part that receives the centrifugal force due to rotation is composed of columnar grains whose crystallographic orientation can be controlled to avoid unwanted movement of dislocations that induces creep damage [1,3,4]. On the other hand, the lower fixed portion is composed of random polycrystalline equiaxial grains to ensure fatigue resistance and low-temperature toughness [1,3,5]. In biomedical implants (Figure 1b), the strength and stiffness must be adjusted appropriately to adapt to the stress field in the actual application *in vivo* to reduce stress shielding of bone, an objective that can be obtained by a convenient crystalline texture. However, such a level of microstructural control is still limited to entire volume and specific processes, that can be expensive as casting processes [4,5], or geometrically limited to flat shapes as in cold rolling followed by annealing process used in steel sheets [1,7].

At the same time, the use of Additive Manufacturing (AM) processes has grown as a solution to produce geometrically complex products (Figure 1) that are not so simple to obtain through other manufacturing processes [8-10]. Furthermore, some variants of AM have shown the capability to induce strong crystalline texture in metallic materials, especially using energy beams and oriented solidification [11-13].

Although the textures obtained by these AM processes are consequences of the adopted procedural parameters, this dependence is not yet adequately established in the literature [6,9,11], which is not yet general in describing the relationship between process variables versus obtained texture.

[1]*Faculdade de Engenharia, Universidade Santa Cecília, UNISANTA, Santos, SP, Brasil.*
[2]*Departamento de Engenharia Metalúrgica e de Materiais, Escola Politécnica da Universidade de São Paulo, PMT-Poli-USP, Universidade de São Paulo, USP, São Paulo, SP, Brasil.*

**Corresponding author: willyank@unisanta.br*

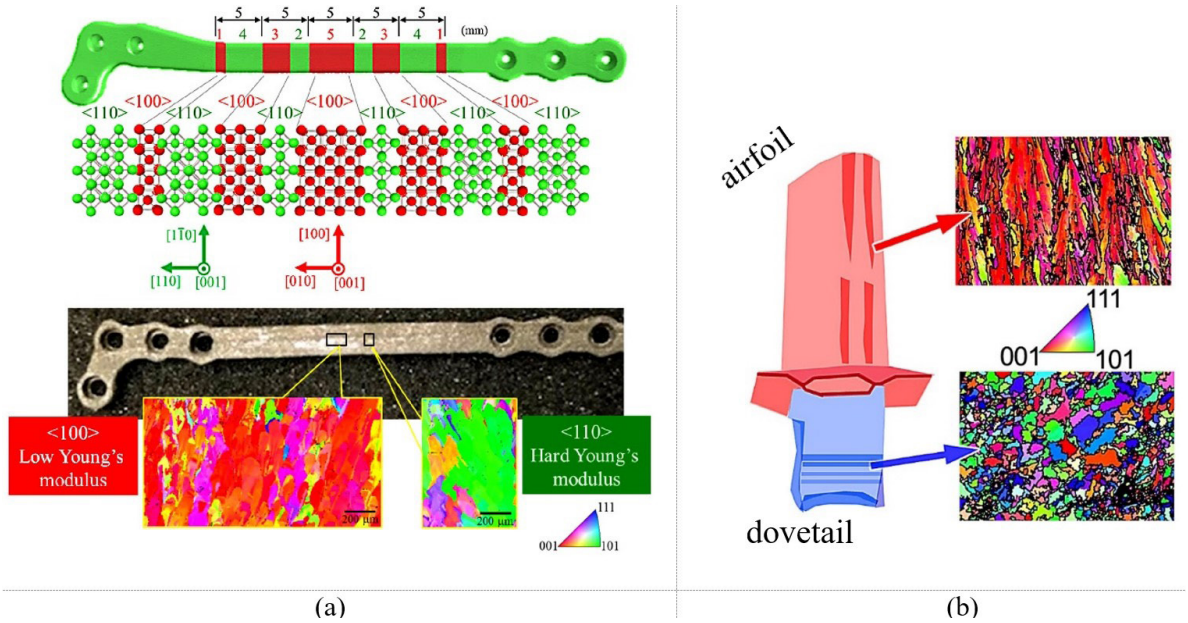

Figure 1. Potential application of crystalline control to increase the performance of metallic components: (a) medical implant adjusted appropriately to adapt to the stress field of bone [6:1768] and (b) turbine blades, with columnar oriented grains in airfoil (up), and equiaxed microstructure in dovetail (down) [6:1771].

Based on this scenario, this review article offers some highlights and trends to explain crystallographic texture control covering AM processes employing laser powder bed fusion (LPBF). The choice of AM by LPBF is justified because this process can not only generate strong textures in metallic products [6,12,13], but also because it is a well-established, highly versatile, and relatively accessible process [9,14,15]. Therefore, AM by LBPF is an important candidate process to control the crystalline texture and, indeed, for the definition of physical and mechanical properties normally not manipulated in metallic products such as stiffness.

2 Crystallographic texture and properties

The great interest in crystallographic texturing lies in the ability to configure, with greater precision or even in an unprecedented way, relevant properties of a crystalline engineering material for a given application [1:231]. Several properties are affected by texture, but the mechanical properties associated with elasticity, strength, ductility, fracture toughness and fatigue are generally the most studied due to their direct importance in engineering applications [2:207]. This is the case of elastic stiffness constants (C_{ij}) or their specific values of Young's modulus (E) for isotropic materials, which are considered practically constant for engineering metals, as they are not easily influenced by traditional manufacturing processes [1:75]; [3:233]. Figure 2 illustrates the dependence of the E value with crystalline directions for selected metals, ordered by increasing anisotropy from W to Cu.

Nevertheless, to obtain relevant effects on stiffness or any other texture-dependent properties is necessary the presence of a strong crystalline alignment [17]. According to Suwas and Ray [2], such a level of orientation is characterized by having at least 30 to 40% of the material formed by crystals ordered in a specific <*uvw*> which can

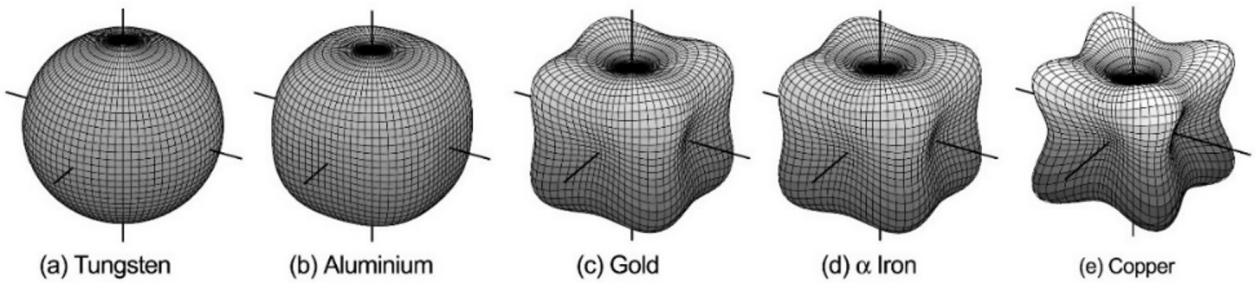

Figure 2. Orientation dependence of Young's modulus (E) with crystalline directions <uvw> for some metals [16:56].

be characterized by the EBSD technique through orientation maps (OMs), or inverted polar figures (IPFs), or (Bunge) Euler angles (φ_1, ϕ, φ_2) [17]. But these tools do not allow extracting a numerical value to quantify the texture level, requiring a more assertive approach, such as using the following Equation 1 [13,18]:

$$P_{\langle uvw \rangle} = \frac{\int_A cos^2\theta_{\langle uvw \rangle} dA}{\int_A dA} \quad (1)$$

Where: $\theta_{<uvw>}$ is the smallest angle between the observation direction and one of the equivalent orientations of <*uvw*>. Under this definition, the value of $\theta_{<uvw>}$ is evaluated at each measured point, and the average value of $\cos^2\theta_{<uvw>}$ by the area (A) of the spherical reference triangle, (defined by the directions [001], [110] and [111]). For example, P<*uvw*>=1 with a perfect alignment and $P_{<100>}$=0.7009; $P_{<110>}$=0.8354 and $P_{<111>}$=0.7577 for randomly oriented polycrystalline cubic structures.

2.1 Solidification texture

Crystallographic texturing can be achieved by combining one or more of the mechanisms [2]:

1. solidification texture, produced by fusion and oriented solidification;
2. deformation texture, that develops by the differential deformation response during forming processes such as rolling, forging, and extrusion;
3. textures of recrystallization and grain growth, formed when deformed material is annealed at sufficiently high temperatures and for prolonged periods and;
4. transformation textures, that originate as a result of crystallographic transformations from an original phase to a final phase.

A manufacturing process will induce strong crystallographic texture when certain solidification conditions occur synergistically. The AM process by LPBF has its texture basically defined by the solidification mechanism [6,9,12], which is the focus of this article. In this case, a strong crystallographic texture comes up when the following conditions occur synergistically like illustrated by Figure 3:

1. induce properly oriented crystals nucleation;
2. forming a continuous structure, consolidated by competitive epitaxial growth due to an alignment with the thermal gradient;
3. remelting crystals of unwanted orientation intensifying the desired texture.

The presence of a low-energy and low-temperature interface or more stable small solid nuclei in contact with the liquid phase gives aid to solidification [4]. Once nucleated, the growth rate of solid crystals depends on the movement of a solid-liquid interface, whose dynamics are dictated by the rate of atoms aggregated [19,20]. Crystalline surfaces that have better conciliation between lower planar density (ρ_p) and availability of stronger bonds will become faster, more stable, and thus priority growth planes during solidification [19]. This situation is particularly aided by the thermal gradient (G), as will be discussed shortly. The aforementioned conditions lead to epitaxy, a type of crystal growth in which new crystalline layers are formed with one or more well-defined preferential orientations concerning the crystalline former layer. Epitaxy crystalline directions <*uvw*> will be defined throughout this article as $D_{<uvw>}$.

For cubic crystalline systems, the {100} family of planes presents both low density and good atomic bond anchorage [19:12]; [21:319]. Therefore, the presence of {100} interfaces can induce epitaxial $D_{<100>}$ growing, especially if there are thermal conditions present favorable to the competitive growth of more stable interfaces. The energy extraction rate or heat flux (Q), which has the same direction, but with the opposite direction to the thermal gradient (G), influences crystalline growth in metals [4,5,22-25].

As shown by Figure 4a, lower thermal transfer (G/R), due to lower temperature gradients (G) and higher growth rates (R) in the liquid, supports a dendritic solidification

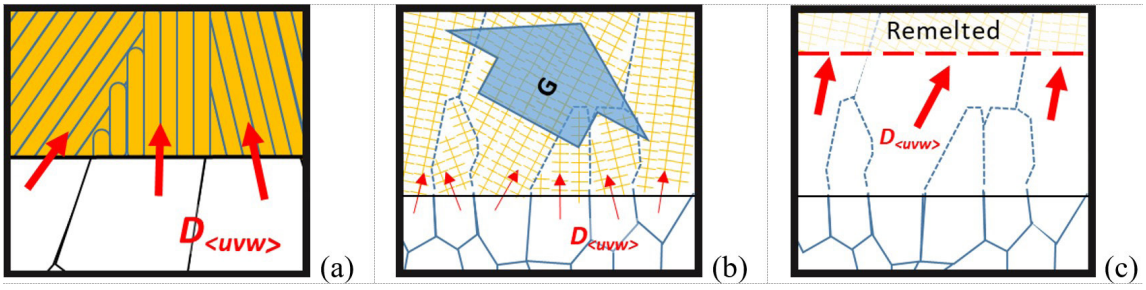

Figure 3. Schematic illustration of three conditions to induce a strong crystalline texture from solidification mechanism based on the sequence: (a) oriented nucleation, (b) competitive columnar growth ($D_{<uvw>}$//G), and (c) proper remelting reinforcing a textured surface/layer.

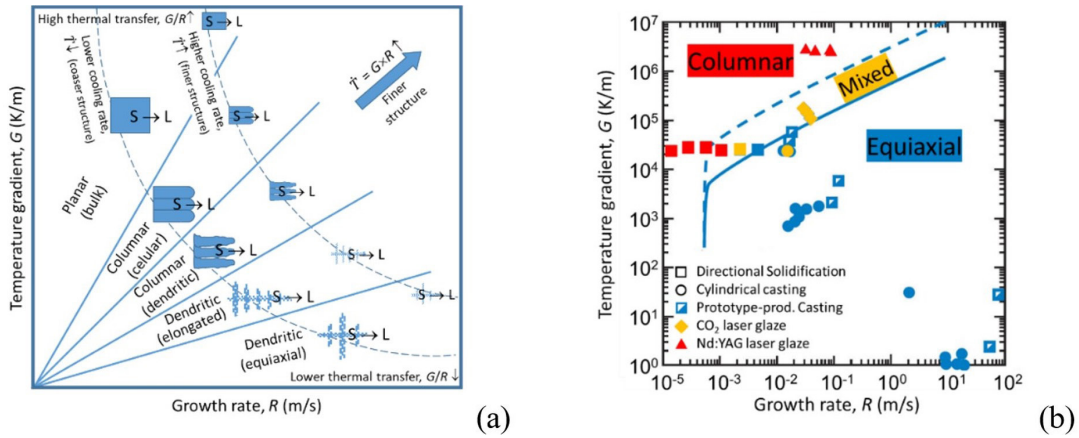

Figure 4. General conditions of crystal formation during solidification, according to a G×R map: (a) general view where G/R (k·s/m^2) determines the morphology and G×R (K/s) determines the size of solidified structure, adapted from Lippold [25] and (b) specific results for Ti-6Al-4V with data from different manufacturing processes, adapted from Collins et al. [11].

process. Contrary conditions lead to the formation of columnar grains with planar or cellular fronts. Additionally, dendritic solidification may exhibit a change in columnar to equiaxed morphology when the G/R ratio is lower, as shown by Figure 4b. Both columnar or dendritic structures fronts grow according to epitaxially preferred directions ($D_{<uvw>}$), which in turn tend to be aligned with the direction of the temperature gradient at the solid-liquid interface. Therefore, for cubic crystal systems, this leads {100} directions to growth parallel to the thermal gradient (G) direction, or $D_{<100>}//G$ as a general trend described in the literature [4,19,24,26,27].

3 Texture in AM by LPBF

The AM by laser powder bed fusion (LBPF), also known as selective laser melting (SLM) or direct metal laser sintering (DMLS) is schematically illustrated in Figure 5 [28]. In this process, a laser beam scans the surface along the so-called Scanning Direction (SD), at a controlled speed (v) and according to a scanning strategy geometry on the powder bed, melting together the particles present to the solid material underneath or by partial melting [selective laser sintering (SLS)]. The powder bed table is lowered by a defined height (t_h) and a new layer of powder is deposited and leveled by a ruler named 'recoater'. The described process is repeated until the part is completely built along the so-called Build Direction (BD).

Moreover, the perpendicular direction to the laser scanning direction is defined as the Transverse Direction (TD) [9,10,14,28]. The three mentioned directions (BD, SD, and TD) are customarily used as a reference coordinate system for the process, as indicated in Figure 5. The great advantages of AM by LPBF are: (1) obtaining complex parts, (2) minimum need of raw material (metallic powder), (3) capability to work with high melting point metals and (4) the possibility to obtain final parts without further complex steps [8-10,15].

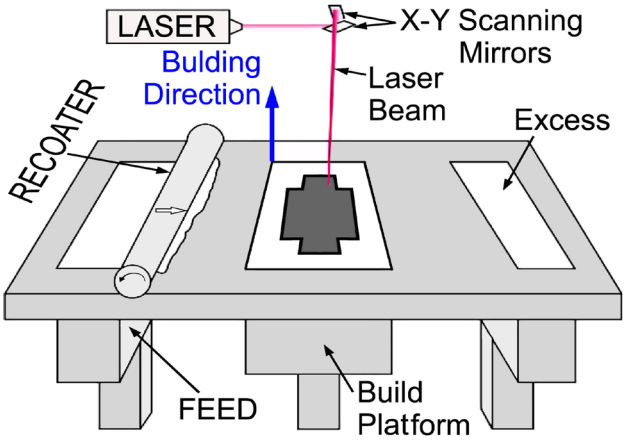

Figure 5. Schematic illustration of the laser-based powder bed fusion process [28:104].

3.1 Process variables

The range of parameters that can be used in AM within which it is possible to obtain an accredited end-use product is known as the "processing window" [9,29]. Traditionally, the processing window is initially defined to obtain a high-density product with scan speed (v) and laser power (P) the basic parameters that define it [2,9,30]. But the exact definition of a processing window depends on the final use in terms of geometric, physical, chemical, structural, and/or mechanical requirements [23,27,29-33].

Due to the large number of variables involved [9,14], there is a wide variety of conditions and parameter combinations that can influence the results obtained in products from AM by LPBF. Therefore, in a previous publication [34], the present authors proposed the grouping of AM by LPBF parameters in four groups of similarities:

1. deposition variables, such as velocity (v), power (P), effective diameter (d_f) of the beam, hatch distance

(h_p) between scans, deposition (t_d) and melted layer thickness (t_m), scan strategies (SS);

2. geometry variables, linked to the geometry of the support structures and to the final product itself;
3. powder variables, linked to the powder-like type (spherical or irregular), surface condition (smooth or rough), reflectance, compaction, dimensional distribution; and
4. metal/alloy variables, such as melting temperature (T_f), *liquidus* (T_L), and *solidus* (T_S) as a function of metal/alloy, thermal conductivity (κ), heat capacity (C_v);
5. general variables, associated with conditions not foreseen in the other groups or secondary, like the chamber atmosphere, type, and temperature of the substrate, and others.

Composite parameters, dimensionless or not, obtained by combining these variables are also used. A widely used parameter to describe AM processes by energy beams is the energy introduced volumetrically by the beam itself (EV) [6,9], as showed by equation (2):

$$E_V = H_L / (h \cdot t) = P / (v \cdot h \cdot t) \quad (2)$$

Where: P (W) is power, v (mm/s) is scan speed, h (mm) is the width between lanes, and t (mm) height of the bed, that defines E_V (J/mm^3) or H_L = P /v (W·mm/s).

There are some criticisms regarding the application of a simple parameter like E_V in different systems. For example, the effective layer deposited (t_d) and melted (t_m) are different from lowered height (t_h), both former are associated not only with the lowering step of the bed table but with the apparent density of the powder, too [35]. Another limitation is the different effects of laser reflection and effective energy absorption in the process, along different metallic systems [36].

3.2 Influence on crystallographic texture

The solidification structure, grain morphology, and orientation (texture) in AM by LPBF are highly dependent both on the metallic system used and the adopted processing conditions [34,37]. Although there is no general rule about which combinations of parameters are most suitable to obtain and control crystallographic texture, the following conditions have been reported by literature as combinations that were able to induce strong crystallographic texture in metallic systems produced with AM by LPBF:

1. molten pool conditions,
2. laser power and scan speed (energy),
3. scan strategy and,
4. other conditions.

3.2.1 Molten pool conditions

As pointed out by literature, LPBF process involves very fast heating, melting, solidification, and cooling phenomena associated with temperature gradients typically around 10^6 K/m [23,34,38,39]. Those mentioned conditions favor the solidification of large columnar (elongated) grains [5,11,23,25,38] especially when bigger G/R ratios are present (Figure 4b). The presence of this microstructure is essential to induce crystalline texture by synergistic epitaxial nucleation and growth between columnar or dendritic elongated grains, a mechanism recurrently reported by literature [9,12-14,32,40-43]. For this mechanism to work, the geometry and dynamics of the molten pool need to match $D_{<uvw>}$ (preferential epitaxial crystalline direction) to the thermal gradient (G) direction, whereas for cubic systems epitaxy occurs when $D_{<100>} // G$ (parallel) or $D_{<100>} \perp G$ (perpendicular) [26,31,44].

Figure 6 presents a simplified planar analysis to explain the association of crystalline texture with different molten pool conditions (G). It can be noted that all three conditions for obtaining strong solidifying texture (Figure 3) are represented in Figure 6: epitaxial (directional) nucleation, competitive (continuous) growth structure, and filtered texture by remelting. In the first condition shown in Figure 6a, the process variables used led to the form of a melt-pool that induces an angular growth between {100} directions with the *BD*. When the laser beam passes to melting the next layer, unmelted grains can maintain their initial angular growth to *BD*. In this case, if this angle is around 54.7° an unusual crystal texture {111}//*BD* can result, as reported by Thijs et al. [13] for tantalum. It is important to highlight that the {111}//*BD* texture is rare in literature, even when the building process starts on a monocrystalline-like surface [18]. This means that such a combination must be unusual.

Likewise, as indicated by Figure 6b, if a flatter molten pool is present, it will induce preferential conditions of parallelism between $D_{<100>}$, G, and *BD*, which leads to the formation of a *BD*-aligned remnant crystalline texture <100>. Garibaldi et al. [31] present this situation, where the degree of concavity of the molten pool influences the texture obtained in samples of high silicon steel produced by SLM. The complexity of the melt pool shape and the dynamics of molten metal can lead to more perturbations in the thermal profile. Cells might initially grow with $D_{<uvw>} // G$, but as they grow to different regions at which a new local G is no longer preferable for the growing cells, side-branching of cells may occur even within a melting pool [44]. Yu et al. [24] warn that the velocity of the liquid inside the molten pool can impair the formation of grains and consequently their epitaxy. The work of Rasch et al. [23] offers some results with Al-Cu alloy demonstrating the possibility to obtain a columnar textured or an unoriented and equiaxial microstructure varying G and R parameters of AM by LPBF.

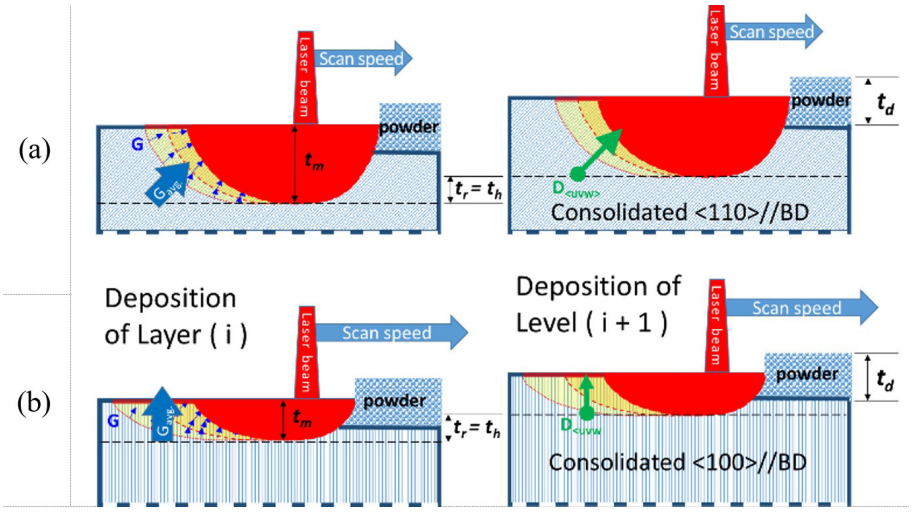

Figure 6. (a) Protuberant and (b) flat sections geometries of the molten pool in *BD*×*SD* plane and their relationship with texture as dictated by G_{avg} // $D_{<uvw>}$: (thickness: t_d - deposition powder, t_m - melted, t_r – remaining and t_h - lowered table level).

3.2.2 Laser power and scan speed

Both the *P* and *v* parameters have traditionally been used to plot process window graphs against porosity or density as done by Majumdar et al. [30]. Therefore, it is natural to try to use these parameters as guiding conditions to obtain crystalline texture in metallic systems produced by LPBF. In fact, most works present their results of crystalline texture as a function of *P* and *v* (or E_v), like in the work by Tsutsumi et al. [45], Sun et al. [46] illustrated by Orientation Maps (OMs) or $P_{<uvw>}$ values as used by Ishimoto et al. [47] and shown in Figure 7. A more general view of this scenario is provided by Hibino et al. [12] and presented in Figure 8. In the latter case, it is worth noting that different textures can be obtained only by the variation of scan speed and not Power (Figure 8).

Despite being tempting, the use of such simple parameters is inaccurate when considering different metallic systems, and therefore the values covered by the bibliography are quite varied. This occurs because each metallic system will present different physical (density, reflectance, thermal conduction, and capacity, etc.) and metallurgical (*liquidus* temperature, crystalline structure, phase stability, and transformation, etc.), as all properties influence the molten pool dynamics (see 2.2.1), including the geometry of the powder particles [48]. Therefore, it is necessary to seek more universal and representative parameters to quantify and describe, comprehensively and assertively, the relationship between procedural conditions, metallic systems, and texturing. However, the adoption and use of such parameters are still limited [34].

3.2.3 Scan strategy

Scan strategy can be described as the way or path through which the laser beam scans the forming layer during LPBF. Their main characteristics are the hatching distance (h_d) or distance between the center of neighboring scan paths, the grouping of the laser path in 'islands' on the surface, track angle between scanning directions (α) and inversion (or not) of direction during deposition on the same layer (between 'islands') or in different level layers. In AM by LPBF, it is common to use different strategies, essentially to reduce residual stresses or porosity [9,44] or to maximize strength by reducing grain size [6,23]. However, his practice also strongly affects the crystalline texture of the material, both in terms of intensity and orientation [6,18,26,44,45,49]. A scan strategy that favors texture may harm other desired characteristics like high strength and low residual stresses, thus making it challenging to reconcile these requirements in AM by LPBF [9,34,37].

Results available from the literature demonstrate the ability of the deposition strategy to intersect the molten pools in order to ensure complete melting of the powder and/or compatibility between the thermal gradients (*G*) of neighboring pools, which are already naturally asymmetric [27,41], with the preferred epitaxial growth directions ($D_{<uvw>}$), as discussed in 2.2.1. Sun et al. [26,46] and Ishimoto et al. [47,49] presented a series of works discussing the influence of scan strategy on crystalline texture on Ni-Mo, Ti-Mo-Zr-Al, and 316L stainless steel alloys. In these studies, it was pointed out that employing correct scanning strategies for each LPBF system is essential to establish crystalline texture. Ishimoto et al. [49] obtained two very different results with Ti-Mo-Zr-Al only by the variation of scan strategy from XX (α=0°) to XY (α=90°): <110>(001) texture with XX and <100>(001) texture with XY.

3.2.4 Other conditions

Other secondary conditions influence the control of the crystalline texture in products made with AM by

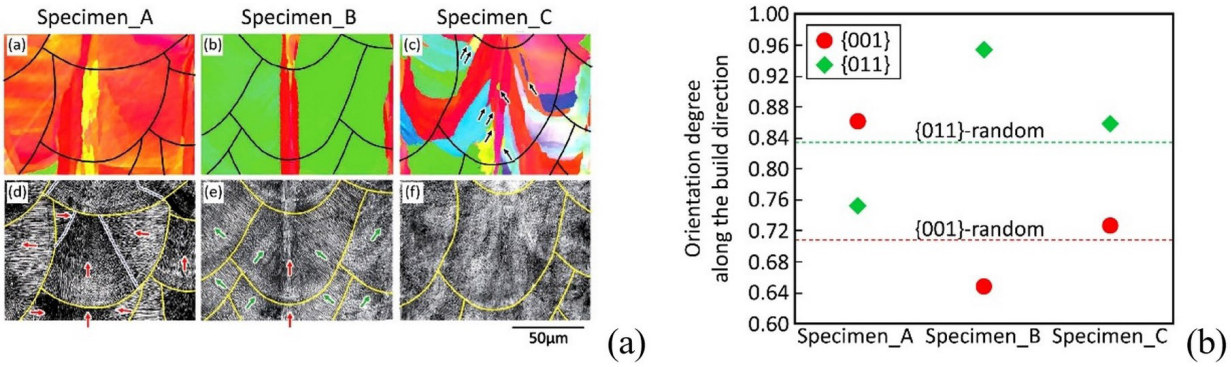

Figure 7. Example of the influence of scan speed on processing conditions that create strong crystalline texture (a) OMs and microstructure (b) $P_{<uvw>}$ values according to Equation 1 [47:4-5]. Scan speed used by specimen: A – "low", B – "medium", and C – "high" (numeric values not available).

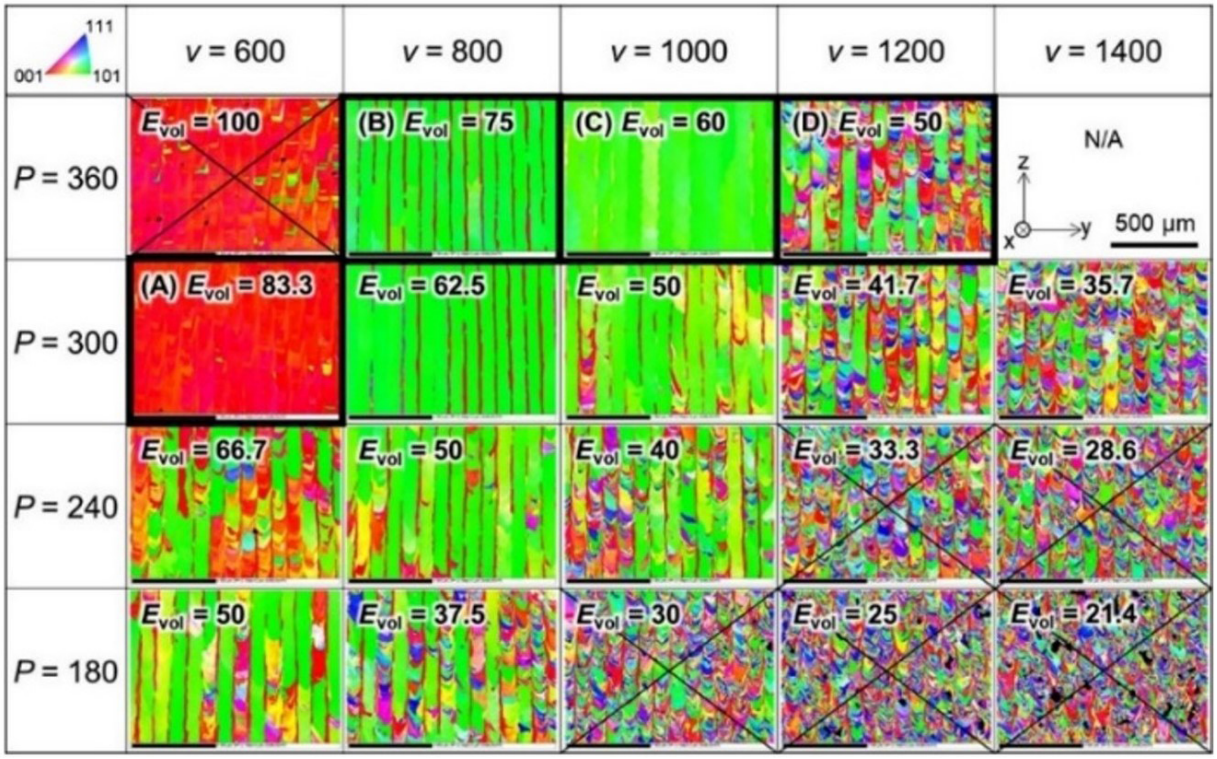

Figure 8. OMs illustrate the strong dependence of crystalline texture with the process variables (P and v) for a nickel alloy (Hastelloy-X) [12:5].

LPBF. One of the most logical is the bulk continuity and/or homogeneity of the thermal history during building. These both are harmed close to scan islands borders [37] or at where transient conditions are present [33] or simply near the lateral and bottom edges of the part [9,27] illustrated by Figure 9 by Light Optical Microscopy (LOM) and Orientation Maps (OMs) for a pure tantalus part built by LPBF [13].

The crystalline orientation of the base substrate or layer on which the part is being built favors to a certain extent the crystalline texture, as demonstrated by Ishimoto et al. [18], where LPBF Ti–15Mo–5Zr–3Al samples were built on monocrystalline substrates ($P_{<uvw>}$=1.0). In that study, even when the most favorable process conditions were applied, the final texture obtained was limited to about $P_{<uvw>} \approx 0{,}90$ as shown by Figure 10a. In contrast, unfavorable construction conditions did not produce immediate random orientation ($P_{<100>}$=0.70 and $P_{<110>}$=0.84) from a monocrystalline substrate, at least along a transient zone as illustrated by Figure 10b. These results suggest that texture and thus stiffness control are limited until a certain range due to process efficiency. This trend to was also obtained by Geiger et al. [50].

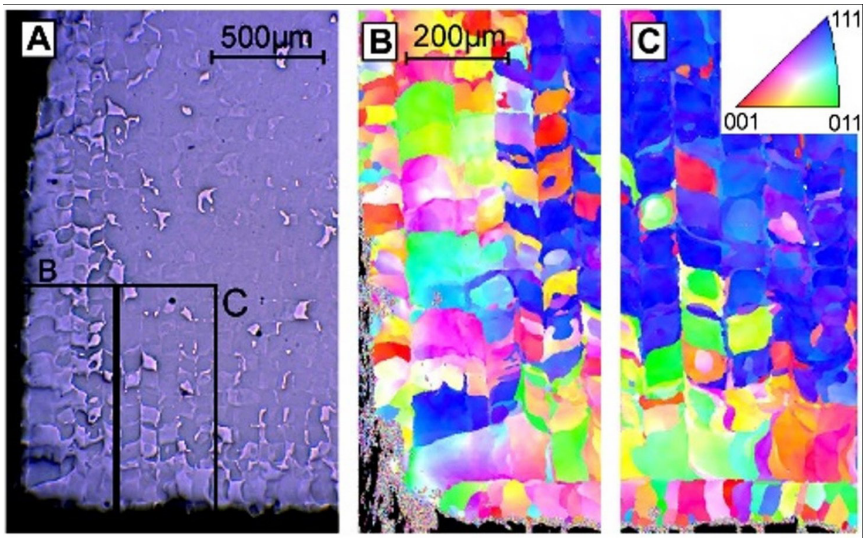

Figure 9. LOM and OMs images of the top face of a pure tantalus part produced by LPBF showing misoriented zones near its edge (crystal orientations along *BD*) [13:4662]. (a) sample as polished; (b) Inverse Pole Figure near edge and (c) continuing the previous image.

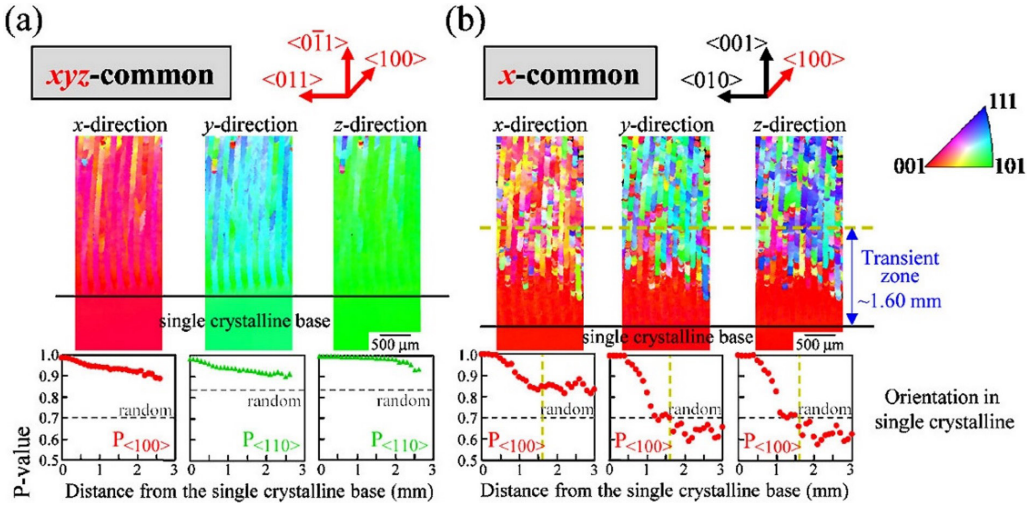

Figure 10. OMs demonstrate the continuity of texture from a monocrystalline substrate ($P_{<uvw>}$=1.0) as a function of LPBF building variables: (a) best condition of texture continuity ($P_{<100>}$ and $P_{<110>}$≈0.90) and (b) worst situation with quasi-random structure (P<100>≈0.70) [18].

The laser beam has some influential role too, not only concerning laser wavelength (λ) and power level (*P*) but also related to how the laser energy is delivered to the powder bed. During AM by LPBF, energy absorption by the powder raw material affects the temperature profiles, molten pool, solidification, and microstructure. Energy absorption depends on the heat source characteristics or the laser power density distribution [9].

Modulated and continuous wave laser beams can be used in AM by LPBF to increase process resolution and reduce residual stresses and overheating [51]. But it impairs the building rate as well as introduces additional variables, like the effective laser power (P_{eff}) [52]. This practice produces different energy inputs to the molten pool, thus altering the microstructure and texture results, as presented by Pham et al. [44] not necessarily improving it. The angle of incidence of the laser beam can change energy input and as pointed out by Young et al. [53]. In this case, more robust conditions are needed to guarantee the stability of oriented grain growth even with variations on incident laser beam angle along all building parts inside LPBF chamber. Pilz et al. [54] point out that a 'top hat' flat laser beam energy profile appears to be very beneficial for the crystalline texture of the beta Ti-Nb alloy. This type of laser led to an improved process stability and build-up rate in relation to a Gaussian laser of the same power.

Finally, Reijonen et al. [43], as well as Young et al. [53], point out that AM by LPBF exhibits other uncertainties, where variations in results are present despite using the same optimized processing parameters. Some of these conditions are the brand

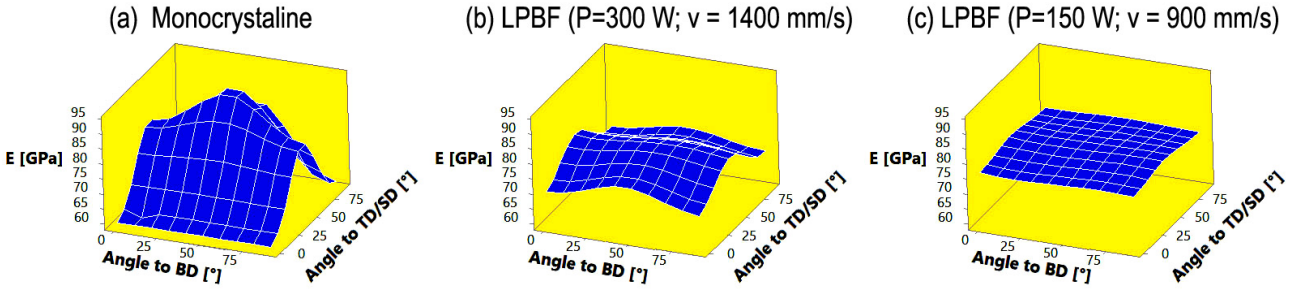

Figure 11. Anisotropy on Young's modulus (*E*) obtained by the present authors with Nb-48Ti alloy as: (a) bulk monocrystalline, (b) LPBF with some texture, and (c) quasi-random LPBF.

and model of the LPBF equipment, chamber size, shielding gas type, flow rate and direction, type of laser return on island boundaries (curved or stopped), size and geometry of the part itself, number of parts being built inside the chamber. Such variables need to be studied on a case-by-case basis and their influence evaluated based on the fundamentals of the process.

4 Some potential applications

AM by LPBF offers the possibility to control mechanical properties by crystallographic texture, which in turn can be designed and obtained through the appropriate choice of process parameters. With the emergence of new production and characterization techniques, as well as new experiments and research, relevant advances in texture control are expected [12,34].

Saghaian et al. [55] demonstrate that the LPBF process can tailoring the microstructure and superelastic behavior of NiTi shape memory alloys.

In this case, the authors employed different local heat transfer of the melt pool by varying hatch spacing to induce changes in the final texture. Higher strain recovery and more stable superelastic behavior were obtained for [001]//BD texture conditions. Sun et al. [46] concentrated only on the mechanism of crystallographic lamellar microstructure (CLM, see Figure 7, specimen_B) development in 316L stainless steel by the X-scan strategy. The authors found that a CLM induced by a low energy density simultaneously improved the mechanical properties and corrosion resistance.

Control of the Young's modulus is strongly desired for the application of metallic alloys as an implant material [49]. A lower stiffness is desired to avoid 'stress shielding', a mechanical incompatibility generated at the contact interface between metallic (stiff) medical implants and bone (mild) tissue [6,56].

Until the moment, some incipient but interesting results of stiffness-induced anisotropy by crystalline texture are presented by Pilz et al. [54], using laser energy profile, and by Geiger et al. [50], using scan strategy and heat treatment. In both works, obtained crystalline texture could induce directions with 34% lower E for Ti-42Nb beta alloys [54], 31% and 8,5% before and after thermal treatment, respectively for Ni-alloy IN738LC [50].

Additionally, Ishimoto et al. [49] obtained different *E* values for samples of Ti–15Mo–5Zr–3Al beta-type alloys manufactured by two different scanning strategies. With XX-scan was obtained E = 68.7 ± 0.9 and 99.6 ± 4.8 GPa and with XY-scan was obtained *E* = 75.3 ± 2.5 and 75.7 ± 1.0 GPa, along BD and TD respectively.

The present authors also obtained some results of E control by texture with Nb-48Ti alloys produced by LPBF. Figure 11 shows a comparison between the results of Young's modulus of Nb-48Ti alloy from (a) theoretical monocrystalline, (b) textured LPBF, and (c) quasi-random LPBF [17,35,37,48]. Although a reduction of only 8% in stiffness was obtained (-6 at 70 GPa), new samples and results are under evaluation.

5 Conclusions

Additive manufacturing (AM) is a process with great potential to generate new applications for engineering materials, as well as induce technological innovations [8-10]. Particularly, AM processes by energy beams, such as laser powder bed fusion (LPBFL) and electron beam (EBPBF), show an aptitude for texture control [3,14,15,40] and, consequently, to obtain desirable unique characteristics in differentiated applications, such as stiffness for medical implants [6,56]. The control of properties by texture in AM processes is still incipient and there is limited knowledge about how the mechanisms that create, and control crystalline texture can be parameterized for AM by LPBF [12,13,18,34,37,54]. This can be justified due to the conjunction of two factors:

1. the great advances, innovations, and diversity of conditions, results, and applications that have been presented recently [9,10,20,28] and
2. the intrinsic procedural complexity, associated with the large number of parameters linked to AM [11,14,32,53].

Nevertheless, the potential for control mechanical properties by texturing is a reality, demonstrated in the literature [37,50,54], and tends to be more assertively sought by researchers.

References

1 Meyers MA, Chawla KK. Mechanical behavior of materials. 2nd ed. Cambridge: Cambridge University Press; 2009.

2 Suwas S, Ray RK. Crystallographic texture of materials. London: Springer-Verlag; 2014.

3 Callister WD Jr, Rethwisch DG. Fundamentals of materials science and engineering: an integrated approach. 5th ed. Versailles: John Wiley & Sons; 2019.

4 Müller A. Solidificação e análise térmica dos metais. Porto Alegre: Editora UFRGS; 2002.

5 Sinha AK. Physical metallurgy handbook. New York: McGraw-Hill; 2003.

6 Hagihara K, Nakano T. Control of anisotropic crystallographic texture in powder bed fusion additive manufacturing of metals and ceramics - a review. JOM. 2022;74:1760-1773. http://dx.doi.org/10.1007/s11837-021-04966-7.

7 Magnabosco AS. Recristalização, crescimento de grãos e textura cristalina. In: Morais WA, Magnabosco AS, Menezes EB No, editors. Metalurgia física e mecânica aplicada. 2nd ed. São Paulo: ABM; 2009. Vol. 1, p. 257-288.

8 Gibson I, Rosen DW, Strucker B. Additive manufacturing technologies - rapid prototyping to direct digital manufacturing. New York: Springer; 2010.

9 DebRoy T, Wei HL, Zuback JS, Mukherjee T, Elmer JW, Milewski JO, et al. Additive manufacturing of metallic components-process, structure and properties. Progress in Materials Science. 2018;92:112-224. http://dx.doi.org/10.1016/j.pmatsci.2017.10.001.

10 Prakash KS, Nancharaih T, Rao VVS. Additive manufacturing techniques in manufacturing - an overview. Materials Today: Proceedings. 2018;5:3873-3882. http://dx.doi.org/10.1016/j.matpr.2017.11.642.

11 Collins PC, Brice DA, Samimi P, Ghamarian I, Fraser HL. Microstructural control of additively manufactured metallic materials. Annual Review of Materials Research. 2016;46:63-91. https://doi.org/10.1146/annurev-matsci-070115-031816.

12 Hibino S, Todo T, Ishimoto T, Gokcekaya O, Koizumi Y, Igashira K, et al. Control of crystallographic texture and mechanical properties of hastelloy-X via laser powder bed fusion. Crystals. 2021;11(9):1064. http://dx.doi.org/10.3390/cryst11091064.

13 Thijs L, Sistiaga MLM, Wauthle R, Xie Q, Kruth J-P, Humbeeck JV. Strong morphological and crystallographic texture and resulting yield strength anisotropy in selective laser melted tantalum. Acta Materialia. 2013;61:4657-4668. http://dx.doi.org/10.1016/j.actamat.2013.04.036.

14 Vrancken B. Study of residual stresses in selective laser melting [PhD thesis]. Heverlee: KU Leuven, Faculty of Engineering Science; 2016.

15 Vlasea ML, Lane B, Lopez F, Mekhontsev S, Donmez A. Development of powder bed fusion additive manufacturing test bed for enhanced real-time process control. In: The University of Texas at Austin. Proceedings of the 34th International Solid Freeform Fabrication Symposium; 2015 Aug 10-12; Austin, USA. Pittsburgh: TMS; 2015. p. 527-539.

16 Roesler J, Harders H, Baeker M. Mechanical behaviour of engineering materials - metals, ceramics, polymers, and composites. Berlin: Springer; 2007.

17 Morais WA, Vasques MT, Nobre RM, Landgraf FJG. Proposta de procedimento para estimar a rigidez em metais texturizados pela análise dos dados de EBSD. Unisanta – Science & Technology. 2020 [cited 2023 Mar 19];9(1):38-45. Disponível em: https://periodicos.unisanta.br/index.php/sat/article/view/2471

18 Ishimoto T, Hagihara K, Hisamoto K, Nakano T. Stability of crystallographic texture in laser powder bed fusion: understanding the competition of crystal growth using a single crystalline seed. Additive Manufacturing. 2021;43:102004. http://dx.doi.org/10.1016/j.addma.2021.102004.

19 Markov IV. Crystal growth for beginners. Singapore: World Scientific; 1995.

20 Zhang J, Song B, Wei Q, Bourell D, Shi Y. A review of selective laser melting of aluminum alloys: processing, microstructure, property and developing trends. Journal of Materials Science and Technology. 2019;35(2):270-284. http://dx.doi.org/10.1016/j.jmst.2018.09.004.

21 Dantizig JA, Rappaz M. Solidification. 2nd ed. Lausanne: EPFL Press; 2009. Dendritic growth; p. 317-384.

22 Fredriksson H, Åkerlind U. Solidification and crystallization processing in metals and alloys. West Sussex: John Wiley & Sons; 2012.

23 Rasch M, Heberle J, Dechet MA, Bartels D, Gotterbarm MR, Klein L, et al. Grain structure evolution of Al-Cu alloys in powder bed fusion with laser beam for excellent mechanical properties. Materials. 2020;13(82):1-22. http://dx.doi.org/10.3390/ma13010082.

24 Yu Y, Wang L, Zhou J, Li H, Li Y, Yan W, et al. Impact of fluid flow on the dendrite growth and the formation of new grains in additive manufacturing. Additive Manufacturing. 2022;55:102832. http://dx.doi.org/10.1016/j.addma.2022.102832.

25 Lippold JC. Welding metallurgy and weldability. New Jersey: John Wiley & Sons; 2015.

26 Sun SH, Hagihara K, Nakano T. Effect of scanning strategy on texture formation in Ni-25at.%Mo alloys fabricated by selective laser melting. Materials & Design. 2018;140:307-316. http://dx.doi.org/10.1016/j.matdes.2017.11.060.

27 Andreau O, Koutiri I, Peyre P, Penot JD, Saintier N, Pessard E, et al. Texture control of 316L parts by modulation of the melt pool morphology in selective laser melting. Journal of Materials Processing Technology. 2019;264:21-31. http://dx.doi.org/10.1016/j.jmatprotec.2018.08.049.

28 Gibson I, Rosen DW, Stucker B. Additive manufacturing technologies: rapid prototyping to direct digital manufacturing. New York: Springer; 2010.

29 Johnson L, Mahmoudi M, Zhang B, Seede R, Huang X, Maier JT, et al. Assessing printability maps in additive manufacturing of metal alloys. Acta Materialia. 2019;176:199-210. http://dx.doi.org/10.1016/j.actamat.2019.07.005.

30 Majumdar T, Bazin T, Ribeiro EMC, Frith JE, Birbilis N. Understanding the effects of PBF process parameter interplay on Ti-6Al-4V surface properties. PLoS One. 2019;14(8):1-24. http://dx.doi.org/10.1371/journal.pone.0221198.

31 Garibaldi M, Ashcroft I, Simonelli M, Hague R. Metallurgy of high-silicon steel parts produced using selective laser melting. Acta Materialia. 2016;110:207-216. http://dx.doi.org/10.1016/j.actamat.2016.03.037.

32 Malekipour E, El-Mounayri H. Common defects and contributing parameters in powder bed fusion AM process and their classification for online monitoring and control: a review. International Journal of Advanced Manufacturing Technology. 2018;95:527-550. http://dx.doi.org/10.1007/s00170-017-1172-6.

33 Yin J, Peng G, Chen C, Yang J, Zhu H, Ke L, et al. Thermal behavior and grain growth orientation during selective laser melting of Ti-6Al-4V alloy. Journal of Materials Processing Technology. 2018;260:57-65. http://dx.doi.org/10.1016/j.jmatprotec.2018.04.035.

34 Landgraf FJG, Morais WA. Considerações quanto à formação de textura cristalina em materiais metálicos produzidos por manufatura aditiva (FLP-L). In: Rede PDIMat. Proceedings of the I Congresso Brasileiro de Engenharia da Rede PDIMat; 2020 Nov 3-5; Natal, Brazil. Natal: UFRN; 2020. p. 584-594.

35 Guzmán J, Nobre RM, Rodrigues DL Jr, Morais WA, Nunes ER, Bayerlein DL, et al. Comparing spherical and irregularly shaped powders in laser powder bed fusion of Nb47Ti alloy. Journal of Materials Engineering and Performance. 2021;30:6557-6567. http://dx.doi.org/10.1007/s11665-021-05916-9.

36 Jodi DE, Kitashima T, Koizumi Y, Nakano T, Watanabe M. Manufacturing single crystals of pure nickel via selective laser melting with a flat-top laser beam. Additive Manufacturing Letters. 2022;3:1-8. http://dx.doi.org/10.1016/j.addlet.2022.100066.

37 Nobre RM, Morais WA, Vasques MT, Guzmán J, Rodrigues DL Jr, Oliveira HR, et al. Role of laser powder bed fusion process parameters in crystallographic texture of additive manufactured Nb-48Ti alloy. Journal of Materials Research and Technology. 2021;14:484-495. http://dx.doi.org/10.1016/j.jmrt.2021.06.054.

38 Bontha S, Klingbeil NW, Kobryn PA, Fraser HL. Thermal process maps for predicting solidification microstructure in laser fabrication of thin-wall structures. Journal of Materials Processing Technology. 2006;178(1-3):135-142. http://dx.doi.org/10.1016/j.jmatprotec.2006.03.155.

39 Promoppatum P, Yao SC, Pistorius PC, Rollett AD. A comprehensive comparison of the analytical and numerical prediction of the thermal history and solidification microstructure of inconel 718 products made by laser powder-bed fusion. Engineering. 2017;3(5):685-694. http://dx.doi.org/10.1016/J.ENG.2017.05.023.

40 Wei HL, Bhadeshia HKDH, David SA, DebRoy T. Harnessing the scientific synergy of welding and additive manufacturing. Science and Technology of Welding and Joining. 2019;24(5):361-366. http://dx.doi.org/10.1080/13621718.2019.1615189.

41 Mukherjee T, Wei HL, De A, DebRoy T. Heat and fluid flow in additive manufacturing - Part II: powder bed fusion of stainless steel, and titanium, nickel and aluminum base alloys. Computational Materials Science. 2018;150:369-380. http://dx.doi.org/10.1016/j.commatsci.2018.04.027.

42 Liu J, To AC. Quantitative texture prediction of epitaxial columnar grains in additive manufacturing using selective laser melting. Additive Manufacturing. 2017;16:58-64. http://dx.doi.org/10.1016/j.addma.2017.05.005.

43 Reijonen J, Revuelta A, Riipinen T, Ruusuvuori K, Puukko P. On the effect of shielding gas flow on porosity and melt pool geometry in laser powder bed fusion additive manufacturing. Additive Manufacturing. 2020;32:1-10. http://dx.doi.org/10.1016/j.addma.2019.101030.

44 Pham MS, Dovgyy B, Hooper PA, Christopher MG, Piglione A. The role of side-branching in microstructure development in laser powder-bed fusion. Nature Communications. 2020;11:1-12. http://dx.doi.org/10.1038/s41467-020-14453-3.

45 Tsutsumi Y, Ishimoto T, Oishi T, Manaka T, Chen P, Ashida M, et al. Crystallographic texture- and grain boundary density-independent improvement of corrosion resistance in austenitic 316L stainless steel fabricated via laser powder bed fusion. Additive Manufacturing. 2012;45:1-9. http://dx.doi.org/10.1016/j.addma.2021.102066.

46 Sun SH, Ishimoto T, Hagihara K, Tsutsumi Y, Hanawa T, Nakano T. Excellent mechanical and corrosion properties of austenitic stainless steel with a unique crystallographic lamellar microstructure via selective laser melting. Scripta Materialia. 2019;159:89-93. http://dx.doi.org/10.1016/j.scriptamat.2018.09.017.

47 Ishimoto T, Wu S, Ito Y, Sun SH, Amano H, Nakano T. Crystallographic orientation control of 316L austenitic stainless steel via selective laser melting. ISIJ International. 2020;60(8):1758-1764. http://dx.doi.org/10.2355/isijinternational.ISIJINT-2019-744.

48 Guzmán J, Nobre RM, Rodrigues DL Jr, Morais WA, Nunes ER, Bayerlein DL, et al. Comparing spherical and irregularly shaped powders in laser powder bed fusion of Nb47Ti alloy. Journal of Materials Engineering and Performance. 2021;30:6557-6567. http://dx.doi.org/10.1007/s11665-021-05916-9.

49 Ishimoto T, Hagihara K, Hisamoto K, Sun SH, Nakano T. Crystallographic texture control of beta-type Ti-15Mo-5Zr-3Al alloy by selective laser melting for the development of novel implants with a biocompatible low Young's modulus. Scripta Materialia. 2017;132:34-38. http://dx.doi.org/10.1016/j.scriptamat.2016.12.038.

50 Geiger F, Kunze K, Etter T. Tailoring the texture of IN738LC processed by selective laser melting (SLM) by specific scanning strategies. Materials Science and Engineering A. 2016;661:240-246. http://dx.doi.org/10.1016/j.msea.2016.03.036.

51 Bruna-Rosso C, Caprio L, Mazzoleni L, Pacher M, Demir A, Previtali B. Influence of temporal laser emission profile on the selective laser melting (SLM) of thin structures. Lasers in Engineering. 2020;47:161-182.

52 Patel S, Vlasea M. Melting modes in laser powder bed fusion. Materialia. 2020;9:1-12. http://dx.doi.org/10.1016/j.mtla.2020.100591.

53 Young ZA, Coday MM, Guo Q, Qu M, Hojjatzadeh SMH, Escano LI, et al. Uncertainties induced by processing parameter variation in selective laser melting of Ti6Al4V revealed by in-situ X-ray imaging. Materials. 2022;15(530):1-17. http://dx.doi.org/10.3390/ma15020530.

54 Pilz S, Gustmann F, Günther F, Zimmermann M, Kühn U, Gebert A. Controlling the Young's modulus of a ß-type Ti-Nb alloy via strong texturing by LPBF. Materials & Design. 2022;216:1-11. http://dx.doi.org/10.1016/j.matdes.2022.110516.

55 Saghaian SE, Nematollahi M, Toker G, Hinojos A, Moghaddam NS, Saedi S, et al. Effect of hatch spacing and laser power on microstructure, texture, and thermomechanical properties of laser powder bed fusion (L-PBF) additively manufactured NiTi. Optics & Laser Technology. 2022;149:1-14. http://dx.doi.org/10.1016/j.optlastec.2021.107680.

56 Elmay W, Patoor E, Bolle B, Gloriant T, Prima F, Eberhardt A, et al. Optimisation of mechanical properties of Ti-Nb binary alloys for biomedical applications. Computer Methods in Biomechanics and Biomedical Engineering. 2011;14(Suppl 1):119-120. http://dx.doi.org/10.1080/10255842.2011.593760.

Received: 19 Oct. 2022
Accepted: 19 Mar. 2023